

1  
2 **Technical Note: On HALOE stratospheric water vapor variations and trends at Boulder,**  
3 **Colorado**

4 **by**

5 **Ellis Remsberg**

6 **Science Directorate**

7 **21 Langley Blvd., Mail Stop 401B**

8 **NASA Langley Research Center**

9 **Hampton, Virginia USA, 23681**

10 **(email: [Ellis.E.Remsberg@nasa.gov](mailto:Ellis.E.Remsberg@nasa.gov))**

11 **Atmospheric Chemistry and Physics Journal**

12 **(June 2023)**

13 **Abstract.** This study compares time series of stratospheric water vapor (SWV) data at 30 hPa  
14 and 50 hPa from 1993 to 2005, based on sets of Halogen Occultation Experiment (HALOE)  
15 profiles above the Boulder, CO (40°N, 255°E) region and on local frost-point hygrometer (FPH)  
16 measurements. Their differing trends herein agree with most of the previously published  
17 findings. FPH trends are presumed to be accurate within their data uncertainties, and there are  
18 no known measurement biases affecting the HALOE trends. However, the seasonal sampling  
19 from HALOE is deficient at 40°N from 2001 to 2005, especially during late winter and  
20 springtime. HALOE time series at 20 hPa clearly show a springtime maximum in SWV at 40°N.  
21 This study finds that the SWV trends from HALOE and FPH nearly agree within uncertainties at  
22 30 hPa, but not at 50 hPa, for the more limited time span of 1993 to 2002. HALOE SWV have  
23 significant and uncertain corrections for interfering aerosol extinction after 1992 at 50 hPa, but  
24 not at 30 hPa. Northern hemisphere time series and daily plots of SWV from the Limb Infrared  
25 Monitor of the Stratosphere (LIMS) experiment indicate that there is transport of filaments of  
26 high SWV from polar to middle latitudes during dynamically active, winter and springtime  
27 periods. Although FPH measurements sense SWV variations at all scales, the HALOE time  
28 series do not resolve smaller-scale structures because its time series data are based on an average  
29 of four or more occultations within a finite latitude/longitude sector. It is concluded that the  
30 variations and trends of HALOE SWV are reasonable at 40°N and 30 hPa from 1993 to 2002 and  
31 in accord with the spatial scales of its measurements and sampling frequencies.

32

33 **1. Background and Objective**

34 There have been numerous studies of long-term changes of stratospheric water vapor (SWV)  
35 mixing ratios (e.g., Konopka, et al., 2022; Hegglin et al., 2014; Hurst et al., 2011). SWV trends  
36 in the lowermost stratosphere are affected mainly by non-zonal variations of the cold-point  
37 temperature (CPT) at the tropical tropopause, followed by transport of the associated relatively  
38 dry, entry-level air. Hegglin et al. (2014) also report on the roles of the oxidation of methane to  
39 water vapor in the middle and upper stratosphere and of changes in the Brewer/Dobson  
40 circulation (BDC) on water vapor trends throughout the stratosphere. One remaining puzzle is  
41 that the SWV trends from frost-point hygrometer (FPH) measurements above Boulder, CO, are  
42 more positive (or less negative) than zonal average and Boulder region analyses of SWV from  
43 the Halogen Occultation Experiment (HALOE) (Scherer et al., 2008). Lossow et al. (2018)  
44 reported that those differences increase with altitude, and they cautioned that trends over Boulder  
45 may not be representative of zonal-mean values some years. Konopka et al. (2022) found from  
46 reanalysis data that there is a moistening above the Boulder region during late boreal winter and  
47 spring.

48

49 The present study reconsiders in Section 2 the HALOE SWV trends and variations near Boulder  
50 for 1993 through 2005 and compares them in Section 3 with those from the Boulder FPH  
51 measurements that are assumed to be accurate. The focus is on the trend differences at 30 hPa,  
52 where Lossow et al. (2018) found that they were largest. Section 4 reports on the SWV trend  
53 differences for the same years at 50 hPa, or where there may be biases in HALOE SWV from its  
54 corrections for interfering aerosols. Section 5 shows a time series of northern hemisphere SWV  
55 near 30 hPa from the Nimbus 7 Limb Infrared Monitor of the Stratosphere (LIMS) dataset of  
56 1978-1979. Daily plots of LIMS geopotential height (GPH) and SWV show the effects of  
57 meridional transport of SWV to 40°N during a dynamically active period in February 1979.  
58 That example provides evidence of a late winter to spring moistening in the Boulder region.  
59 There are also instances of elevated SWV in the HALOE time series at subpolar latitudes at that  
60 time of year. Section 6 concludes that the HALOE SWV variations and trends at 40°N are  
61 understandable compared with those from FPH, given the spatial scales of their measurements,

62 the reduction in sampling by HALOE after 2001, and possible HALOE SWV biases from  
63 interfering aerosols.

64

## 65 **2. Time series analyses of HALOE SWV near Boulder**

66 SWV time series from the HALOE dataset are analyzed by multiple linear regression (MLR)  
67 techniques in the manner of Remsberg (2008) and Remsberg et al. (2018a). Although HALOE  
68 began operations in October 1991, its SWV profiles are degraded in the lower stratosphere in  
69 1991 through mid-1992 because of solar tracking anomalies in the presence of the very large  
70 extinction effects from Pinatubo aerosols. Figure 1a shows HALOE time series data from late  
71 1991 through 2005 for the Boulder sector.

72

73 The Boulder region HALOE SWV points of Fig. 1a are for 30 hPa and are based on averages of  
74 profiles within the latitude range of  $40\pm 4^\circ\text{N}$  and the longitude range of  $255\pm 35^\circ\text{E}$ , since HALOE  
75 seldom measured profiles at the exact location of Boulder. A rather narrow latitude range was  
76 chosen for this study because there is a significant latitudinal gradient in SWV near  $40^\circ\text{N}$  in both  
77 fall and springtime. The finite longitude range of  $\pm 35^\circ$  attains four or more profiles, most times,  
78 from the SR or SS orbital crossings near Boulder, and it is sufficient for indicating low zonal  
79 wavenumber effects on the SWV field. The data in Fig. 1a from January 1993 onward are fit  
80 with an MLR model that corrects for effects of lag-1 autoregression (AR1) and accounts for  
81 memory between adjacent data points (Tiao et al., 1990); its AR1 coefficient is 0.35. The MLR  
82 model fit to the data of January 1993 through 2005 (solid curve) includes constant and linear  
83 trend terms plus periodic annual (AO), semiannual (SAO) and QBO-like terms. The periodic  
84 QBO-like term is approximated as a 28-mo cycle, based on a Fourier analysis of an initial time  
85 series residual after accounting for the seasonal terms. The model also contains proxy terms for  
86 El Nino/Southern Oscillation (ENSO) forcings and solar cycle flux forcings. Significant terms  
87 are SAO, QBO-like, and ENSO proxy; the latter two terms account for differences from the fit of  
88 the HALOE data in Fig. 1a versus that from a simple seasonal fitting. The dashed line in Fig. 1a  
89 represents the sum of the constant term (4.84 ppmv) and a linear trend coefficient of  $-0.22\pm 0.04$   
90 ppmv/decade, having a confidence interval (CI) of 95% or a trend of  $-4.5\pm 0.6(2\sigma)$  %/decade.

91 The SWV trend from Fig. 1a agrees closely with previous trends from HALOE data near 30 hPa  
92 in the latitude range of 35°N to 45°N (Davis et al., 2016; Lossow et al., 2018).

93

94 All MLR term coefficients are reasonably accurate, if the seasonal sampling is good. Yet, there  
95 are indications that HALOE SWV in Fig 1a is larger for sunrise (SR) than for sunset (SS)  
96 occultations from 2002 through 2005. Those differences are because HALOE was turned on  
97 later following a UARS yaw maneuver and turned off a bit earlier prior to the next yaw event, to  
98 conserve power on the UARS spacecraft in late 2001. That change in operating procedure meant  
99 that there were fewer HALOE SR measurements near 40°N during late winter and springtime  
100 after 2001, although it remained good at lower latitudes (not shown). HALOE SWV for the  
101 longitude sector of Boulder but at the higher latitude zone of  $55\pm 10^\circ\text{N}$  is shown in Figure 1b,  
102 where the seasonal sampling is also better compared to that at 40°N in Fig. 1a. Note that  
103 HALOE SWV in Fig. 1b has rather high values in early 2002 or following stratospheric warming  
104 events in the winter of 2001-2002 (Charlton and Polvani, 2007). It may be that there was also  
105 transport of high SWV to 40°N at that time, but HALOE did not observe it directly.

106

107 The negative HALOE SWV trend in Fig. 1a is affected by the downward shift in SWV values  
108 from 2002 onward, as noted by Randel et al. (2006), Scherer et al. (2008), Hegglin et al. (2014),  
109 and Konopka et al. (2022) according to the decrease in SWV in the tropical lower stratosphere in  
110 early 2001. They reported that there was a delay in the decrease of SWV at 40°N because of the  
111 slow ascent of the dry tropical air plus the subsequent meridional transport and mixing of that air  
112 to middle latitudes. Scherer et al. (2008) also noted that it is perhaps more appropriate to apply  
113 two, piecewise linear trend terms for the MLR modeling of the HALOE SWV data in Fig. 1a,  
114 where there is a break point in 2002. Thus, Figure 1c shows a separate trend analysis of HALOE  
115 SWV for the Boulder sector at 40°N, but for 1993 to 2002; its average SWV value is 4.62 ppmv  
116 and its shorter trend term is no longer negative but positive at  $0.22\pm 0.04$  ppmv/decade (or  
117  $4.7\pm 0.7(2\sigma)$  %/decade). Finally, Figure 2 is the residual (data minus MLR model curve) for the  
118 fit in Fig. 1a, and its variations about the mean are of order  $\pm 0.3$  ppmv. An important test of the  
119 adequacy of the set of terms in its MLR model is whether any structure remains in the residual.

120 No periodic structure is apparent in Fig. 2, even though there are clear seasonal gaps in the data  
121 series after 2001.

122

### 123 3. Time series of FPH measurements of SWV

124 Figure 3a is the SWV time series at 30 hPa from the FPH data at Boulder and for 1993-2005 for  
125 comparison with Fig. 1a. Individual FPH profiles were interpolated vertically to obtain SWV  
126 values at the 30-hPa level, and the FPH time series points are also spaced irregularly. SAO,  
127 QBO, ENSO, and Linear terms from the MLR model of Fig. 3a have a significance of better than  
128 90%. The constant term is 4.70 ppmv, which is a bit less than that from the HALOE series (4.84  
129 ppmv) but within the estimated systematic uncertainties for both measurements. The FPH trend  
130 for 1993-2005 is positive or  $+0.17 \pm 0.07$  ppmv/decade (or  $+3.6 \pm 1.5$  ( $2\sigma$ ) %/decade), as compared  
131 to the negative trend from HALOE ( $-4.5 \pm 0.6$  ( $2\sigma$ ) %/decade). There is also a change in trend  
132 around 2002 in the FPH data of Fig. 3a, although it is not so apparent because of the rather large  
133 scatter of the FPH points. Figure 3b shows the corresponding FPH MLR analysis for 1993 to  
134 2002, which yields an average SWV of 4.62 ppmv and agrees with the average HALOE value  
135 from Fig. 1c. The FPH trend for 1993 to 2002 is  $+0.32 \pm 0.6$  ppmv/decade (or  $+6.9 \pm 1.2$   
136 %/decade), which is more positive than that of HALOE ( $+4.7 \pm 0.7$  %/decade) but only slightly  
137 outside the overlapping envelope (e.g.,  $+5.7$  versus  $+5.4$  %/decade) from their mutual trend  
138 uncertainties.

139

140 Figure 4 shows the residual (FPH minus MLR) for the time series data of Fig. 3a, where the FPH  
141 points exhibit more scatter compared with the HALOE residual in Fig. 2. Data points of the FPH  
142 record are assumed to be valid and accurate to  $<6\%$  or about  $\pm 0.3$  ppmv, according to the  
143 extensive studies of Hall et al. (2016). The rather large scatter in Fig. 4 exceeds that uncertainty.  
144 Local FPH measurements are sensitive to SWV variations across all spatial scales. Note that the  
145 structure in the FPH residual of Fig. 4 is aperiodic and presumably due to small-scale  
146 atmospheric variations in some instances. Accordingly, it is difficult for the MLR modeling to  
147 fit all the real structure in the FPH data, and its linear trend term is not highly significant.  
148 Conversely, each individual HALOE profile gives an SWV value that is an average across its

149 tangent view path (~300 km) and with a vertical resolution of no better than two kilometers. The  
150 HALOE time series points are also based on sector averages of four or more profiles. Thus,  
151 HALOE does not resolve SWV variations at small to intermediate scales.

152  
153 There are high FPH SWV values in Fig. 3 on 22 May (5.8 ppmv) and on 26 June 1996 (5.5  
154 ppmv), possibly due to elevated SWV in filaments of polar vortex air that were transported to  
155 and remained isolated above the location of Boulder for days to weeks (e.g., Manney et al.,  
156 2022). A search of individual profiles from HALOE reveals SWV values of order 6.5 ppmv at  
157 60°N, 270°E in mid-March 1996. Temperature at that higher latitude location is only 200 K and  
158 methane is only 0.4 ppmv, both of which are characteristic of winter vortex air. HALOE also  
159 found a small region of high SWV (~5.8 ppmv) and low methane in several soundings near  
160 44°N, 170°E on 12 May 1996. In another instance, FPH has high SWV on 12 April 2000 (5.9  
161 ppmv). HALOE SWV approached 7.0 ppmv near 60°N, 270°E about a month earlier on 18  
162 March 2000; there are also several HALOE values greater than 5.0 ppmv at 40°N on 20 April  
163 2000. An example of a source of the elevated SWV is considered in Section 5.

164

#### 165 **4. Uncertainties for the HALOE SWV trends**

166 Gordley et al. (2009) reported that there are no indications of an instrument bias for the HALOE  
167 SWV trends. However, HALOE SWV profiles may be affected by residual effects from cloud  
168 tops and subvisible cirrus, as shown for HALOE ozone (Bhatt et al., 1999). As a result, the  
169 HALOE SWV trends at pressure levels of 100 hPa and even 70 hPa may not be accurate.  
170 Harries et al. (1996) reported that a given HALOE SWV profile is uncertain by 8% at 40 hPa  
171 because of interfering aerosols, and Hervig et al. (1995) made significant aerosol corrections for  
172 the retrieval of HALOE SWV at 30 hPa and, especially at 50 hPa, following the Pinatubo  
173 eruption. Figure 5 is the HALOE time series at 50 hPa; note that the abrupt decrease of SWV  
174 occurs in mid-2001. While the HALOE trend is negative from 1993 to 2005, the MLR model fit  
175 is positive from December 1992 to mid-2001. Its SAO, AO, QBO, and ENSO terms are  
176 significant, its mean value is 4.28 ppmv, and its trend to mid-2001 is  $+3.7 \pm 1.4$  %/decade.

177

178 Figure 6 is the corresponding FPH time series at 50 hPa. It shows no clear change in 2001,  
179 largely a consequence of the scatter in the data. Its mean value from late 1992 to mid-2001 is  
180 4.21 ppmv, but its trend is  $+10.8 \pm 1.7$  %/decade or much larger than from HALOE. The HALOE  
181 versus FPH trend difference at 50 hPa is qualitatively like that from Scherer et al. (2008, their  
182 Fig. 7). On the other hand, at 30 hPa HALOE has lower aerosol extinction values and yields a  
183 SWV trend for 1993 to 2002 that agrees more nearly with that of FPH (HALOE from Fig. 1c is  
184  $+4.7$  %/decade and FPH from Fig. 3b is  $+6.9$  %/decade).

185

186 Corrections to SWV from interfering aerosols are more significant and extend for longer times at  
187 50 hPa than at 30 hPa. Aerosol extinction profiles are determined from wavelengths of the  
188 HALOE gas filter correlation channels of HF, HCl, CH<sub>4</sub>, and NO (Hervig et al., 1995). Then,  
189 corrections for the HALOE radiometer channels (H<sub>2</sub>O, NO<sub>2</sub>, and O<sub>3</sub>) are a modeled extrapolation  
190 with wavelength from the NO channel aerosol profile at 5.26 micrometers. Example  
191 comparisons of retrieved HALOE SWV versus correlative measurements indicate that the  
192 modeled corrections are qualitatively correct, even in 1992 (Hervig et al., 1996). Nevertheless,  
193 the model for aerosol absorption versus wavelength assumes a size distribution shape and an  
194 aqueous sulfuric acid composition (i.e., refractive index) that is constant with altitude and over  
195 time. Effectively, the aerosol corrections represent a change in aerosol number density only.  
196 That correction model was employed for both a background aerosol layer, as well as for the  
197 decay of the Pinatubo aerosol layer. Thus, there can be a residual, time dependent bias for  
198 HALOE SWV due to the aerosol correction model. Perhaps HALOE SWV is under corrected at  
199 50 hPa for the effects of aerosols through the mid-1990s.

200

201 HALOE SWV trends should be more accurate above the aerosol layer. As a check on that  
202 likelihood, Figure 7 shows the corresponding fit of the HALOE SWV time series from 1993 to  
203 2002 at 20 hPa, or just above the top of the volcanic aerosol layer. SWV has a positive vertical  
204 mixing ratio gradient with altitude, due to the oxidation of methane to SWV in the middle  
205 stratosphere, and average SWV at 20 hPa is 4.74 ppmv or a bit higher than that at 30 hPa (4.62  
206 ppmv). A combined AO/SAO maximum shows clearly in Fig. 7, where the AO amplitude is  
207 twice that of the SAO and the AO and SAO phase maxima are on 19 February and 9 April,

208 respectively. Those cycles confirm the late winter/early spring moistening found in reanalysis  
209 data at 40°N by Konopka et al. (2022).

210

211 The HALOE SWV trend at 20 hPa for 1993-2002 is  $+6.9 \pm 0.9$  ( $2\sigma$ ) %/decade, which agrees with  
212 that at 30 hPa from FPH ( $+6.9 \pm 1.2$  %/decade). (There are too few FPH data at 20 hPa for a  
213 direct trend comparison with HALOE.) Yet, the HALOE trend at 20 hPa is significantly more  
214 positive than its trend at 30 hPa ( $+4.7 \pm 0.7$  %/decade). Remsberg (2015, Table 1) reported  
215 significant positive trends for HALOE methane in the tropical middle stratosphere of order  
216 10%/decade, a small fraction (certainly less than half) of which may have undergone an  
217 oxidization to SWV and subsequent transport to 40°N. The increase of 2.2%/decade for the  
218 HALOE SWV trend from 30 to 20 hPa could be due to that process alone. Thus, it may be that  
219 the HALOE aerosol corrections at 30 hPa are reasonable over time.

220

## 221 **5. Source for the springtime moistening at 40°N**

222 Hegglin et al. (2014) and Remsberg (2015) showed that both methane and water vapor from  
223 limb-viewing satellite datasets (SPARC, 2017) are good indicators of seasonal variations of the  
224 BDC in the stratosphere. They reported on a hemispheric asymmetry for the net circulation,  
225 where the BDC in the northern hemisphere (NH) is stronger and its methane and relative SWV  
226 trends are more positive than in the southern hemisphere. The strength of the NH BDC is  
227 enhanced in winter, primarily due to effects of forcings from planetary waves. There is chemical  
228 conversion of methane to water vapor in the middle and upper stratosphere followed by descent  
229 of that relatively moist air to the lower stratosphere in the region of the polar vortex.

230

231 Seasonal SWV data from the LIMS experiment illustrate the above process for 1978-1979.  
232 Figure 8 (from Remsberg et al., 2018b, their Fig. 14) displays a seasonal increase in SWV within  
233 the NH on the 550 K potential temperature surface (near 30 hPa) in terms of its area diagnostic  
234 versus equivalent latitude, which is a vortex-centered display of SWV along potential vorticity  
235 contours. Fig. 8 indicates that enhanced values of water vapor descended to this surface in the  
236 vortex region by early January and continued through March. Specifically, there was an



237 equatorward expansion of the average SWV value of 5.2 ppmv to the equivalent latitude of 40°N  
238 during mid-February and from mid-March onward, as the high latitude air mixed with lower  
239 latitude air. Note that the 550 K surface is well above the tropical tropopause, minimizing  
240 effects due to any meridional exchanges of water vapor within the lowermost stratosphere.  
241 Similar analyses of seasonal changes of ozone also show that there is further descent to lower  
242 potential temperature levels during springtime and a similar transport and mixing of polar air to  
243 lower latitudes at those levels (Curbelo et al., 2021).

244

245 Polar plots of LIMS Version 6 (V6) geopotential height (GPH) and SWV for 17 February 1979  
246 are in Figures 9 and 10. They indicate the effects of meridional transport of polar air to middle  
247 latitudes, in response to a high latitude, zonal wave-2 event. Fig. 9 shows high GPH (and  
248 anticyclonic circulation) in the Aleutian and eastern Atlantic sectors and low GPH in the polar  
249 vortex (cyclonic) that extends southward across North America. The associated higher values of  
250 SWV in Fig. 10, though somewhat noisy, are characteristic of vortex air that also underwent a  
251 southward transport. The vortex (region of highest SWV) is elongated and extends equatorward  
252 around 90°E and 270°E. There is also a filament of high SWV (>5.5 ppmv) at the latitude of  
253 Boulder and across adjacent longitudes. The seasonal time series display of NH SWV in Fig. 8  
254 shows that this is when the 5.2 ppmv contour extends to near 40°N equivalent latitude.

255

256 Figure 8 also indicates that there was an initial descent of polar air with higher values of SWV to  
257 near the 31.6 hPa surface around 10 January. Then there was a more general expansion of  
258 elevated SWV to the equivalent latitude of 40°N by the end of January (follow the 4.8 ppmv  
259 contour in Fig. 8). Similar instances of meridional transport and mixing to North American  
260 middle latitudes are a likely cause of the sporadic appearance of high SWV values during the  
261 winter and early spring seasons of the FPH measurements in Fig. 3 and in the recent reanalysis  
262 studies of Konopka et al. (2022) and of Wargan et al. (2023). However, the HALOE time series  
263 points in Fig. 1 do not resolve such features so well because they are based on averages of four  
264 or more profiles from within the rather large sector around Boulder.

265

266 HALOE SWV time series were also analyzed for occurrences of higher SWV in three separate  
267 longitude sectors (North America,  $255\pm 35^\circ\text{E}$ ; Aleutian,  $180\pm 35^\circ\text{E}$ ; and European,  $35\pm 35^\circ\text{E}$ )  
268 from 1993 to 2002. There are several such instances at  $40^\circ\text{N}$  in the Boulder sector (Fig. 1), but  
269 none in the Aleutian or European sectors (not shown). Conversely, Figure 11 shows that there  
270 are several positive SWV anomalies within the higher latitude zone of  $53\pm 7^\circ\text{N}$  in the European  
271 sector but none in the Boulder or Aleutian sectors (not shown). SWV in Fig. 11 approaches 6.0  
272 ppmv in four instances (on 22 April 1994, 14 April 1996, 7 March 2000, and 14-19 February  
273 2001), and average SWV is 5.14 ppmv. All four instances are accompanied by low values of  
274 methane, which is a tracer of the transport of polar air to lower latitudes. The instances in 2000  
275 and 2001 also occurred just after temperatures in the upper stratosphere were of order 270 K or  
276 like that for a sudden stratospheric warming (SSW) event. There was a rather extended area of  
277 higher SWV over Europe, not merely a filament of vortex air, following those events.

278

## 279 **6. Summary and Conclusions**

280 Analyses of time series of HALOE and FPH SWV were conducted at 30 hPa and 50 hPa for the  
281 Boulder region. Sampling frequencies for both sets of time series are of the order of a few days  
282 to several weeks. The SWV trend in the Boulder region is positive from the FPH and negative  
283 from the HALOE data from 1993 to 2005. It is assumed that the time series of FPH SWV  
284 measurements are accurate, or to within their uncertainties of  $<6\%$ ; the foregoing HALOE/FPH  
285 trend differences appear significant. However, there are rather large gaps at  $40^\circ\text{N}$  during late  
286 winter and spring in the HALOE time series after 2001, due to the limited power that was  
287 available for HALOE operations. This makes it is more difficult to resolve the seasonal terms  
288 and the trend term from HALOE data after 2001.

289

290 The HALOE SWV trend goes from positive to negative around 2002, and that change is a  
291 delayed effect following the sharp decrease in tropical, lower stratospheric SWV that occurred  
292 early in 2001. The FPH time series has a trend that is less positive after 2001, too, although that  
293 change is not so obvious because of the larger scatter for its points. It is more appropriate to fit  
294 two, piecewise linear trends to both the HALOE and FPH time series with a break point in 2002.

295 There are no known measurement biases that are affecting the HALOE trends. However, the  
296 retrievals of HALOE SWV do have significant and uncertain corrections for interfering aerosol  
297 extinction following the eruption of Pinatubo, particularly at 50 hPa, where the trends from  
298 HALOE and FPH disagree. The analyzed HALOE trend ( $+4.7\pm 0.7$  %/decade) at 30 hPa agrees  
299 more closely with that from FPH ( $+6.9\pm 1.2$  %/decade), or where the aerosol corrections are  
300 relatively small after 1992.

301

302 The HALOE SWV time series at 20 hPa clearly shows a springtime maximum. Northern  
303 hemisphere SWV time series from the Limb Infrared Monitor of the Stratosphere (LIMS)  
304 experiment indicate a transport of higher SWV from polar to middle latitudes during late winter  
305 and springtime. Daily surface maps of LIMS SWV reveal filamentary structure at the latitude of  
306  $40^{\circ}\text{N}$  during and following dynamically active periods. Surface maps of GPH verify that there  
307 was meridional transport of high SWV from the polar vortex to the latitude of  $40^{\circ}\text{N}$  at those  
308 times. Whereas FPH measurements sense SWV variations at all scales, the HALOE time series  
309 do not resolve intermediate to smaller scale structure because its data points are based on an  
310 average of four or more occultation profiles within a finite latitude/longitude sector centered on  
311 Boulder. It is concluded that the variations and trends of HALOE SWV are reasonably accurate  
312 at  $40^{\circ}\text{N}$  and 30 hPa for 1993 to 2002 and in accord with the spatial scales of its measurements  
313 and its sampling frequencies.

314

### 315 **Data Availability**

316 The LIMS V6 Level 3 product and the HALOE V19 profiles are at the NASA EARTHDATA  
317 site of EOSDIS and its Website as:

318 [https://disc.gsfc.nasa.gov/datacollection/LIMSN7L3\\_006.html](https://disc.gsfc.nasa.gov/datacollection/LIMSN7L3_006.html), and as

319 [https://disc.gsfc.nasa.gov/datacollection/UARHA2FN\\_019.html](https://disc.gsfc.nasa.gov/datacollection/UARHA2FN_019.html), respectively.

320 Frost point hygrometer (Lev) data were downloaded from the NOAA website:

321 [https://gml.noaa.gov/aftp/data/ozwv/WaterVapor/Boulder\\_New/](https://gml.noaa.gov/aftp/data/ozwv/WaterVapor/Boulder_New/).

322

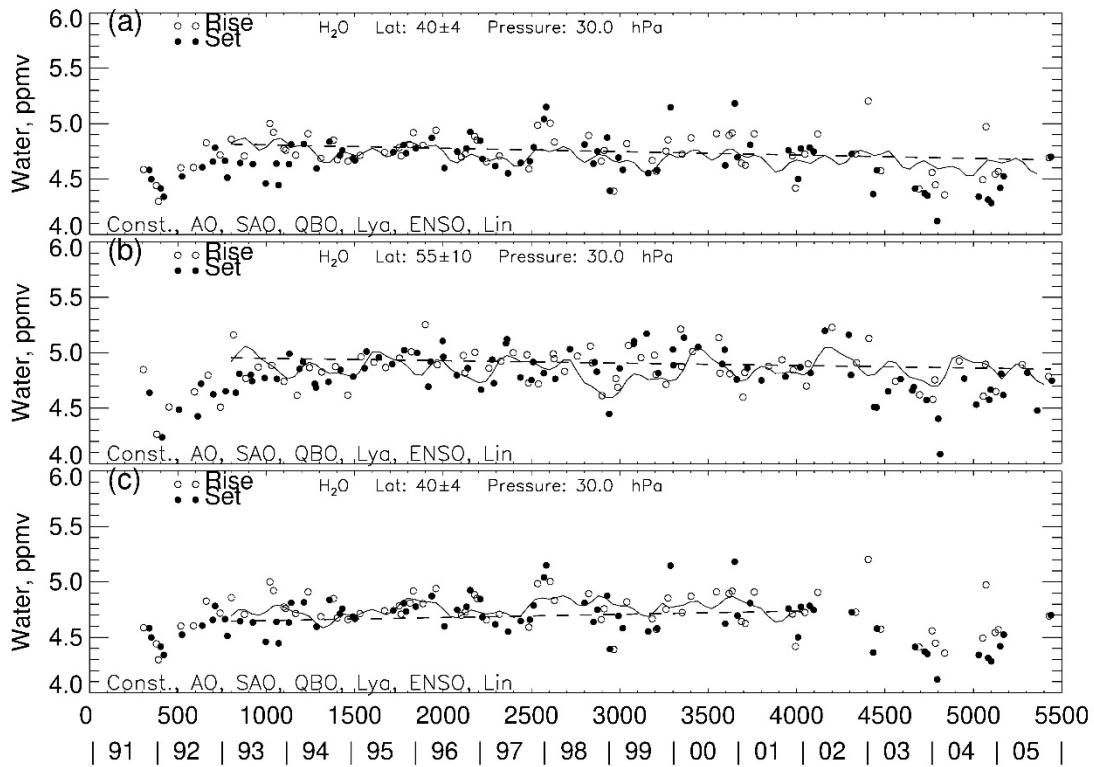
323 *Competing interests:* The author declares no competing interests.

324

325 *Acknowledgements.* Author EER thanks V. Lynn Harvey for generating the plot in Figure 8 that  
326 appeared originally in Remsberg et al. (2018b). EER also appreciates comments by Mark Hervig  
327 on a draft of the manuscript. EER carried out this work while serving as a Distinguished  
328 Research Associate of the Science Directorate at NASA Langley.

329

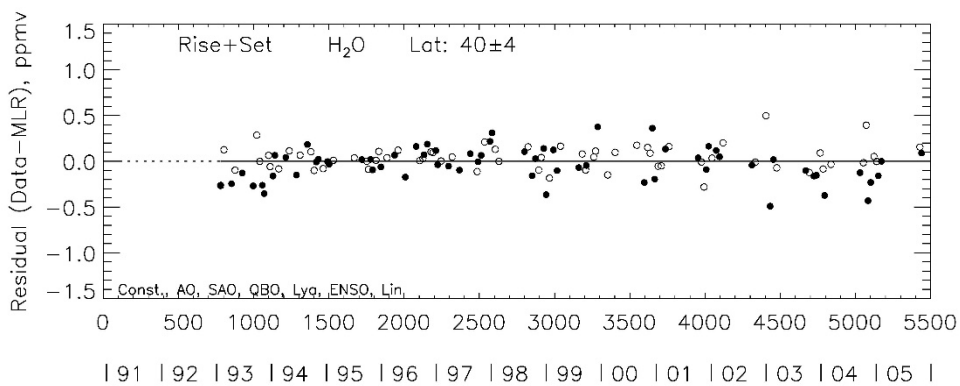
330



332

333 Figure 1—MLR fit to a HALOE SWV time series; (a) Boulder sector, 40°N, 1993-2005, (b) at  
 334 55°N, and (c) 40°N, 1993-2002. The fit of all the MLR terms is the oscillating curve; the linear  
 335 trend term is the straight dashed line. Time by year or in days on abscissa begins Jan. 1, 1991.

336

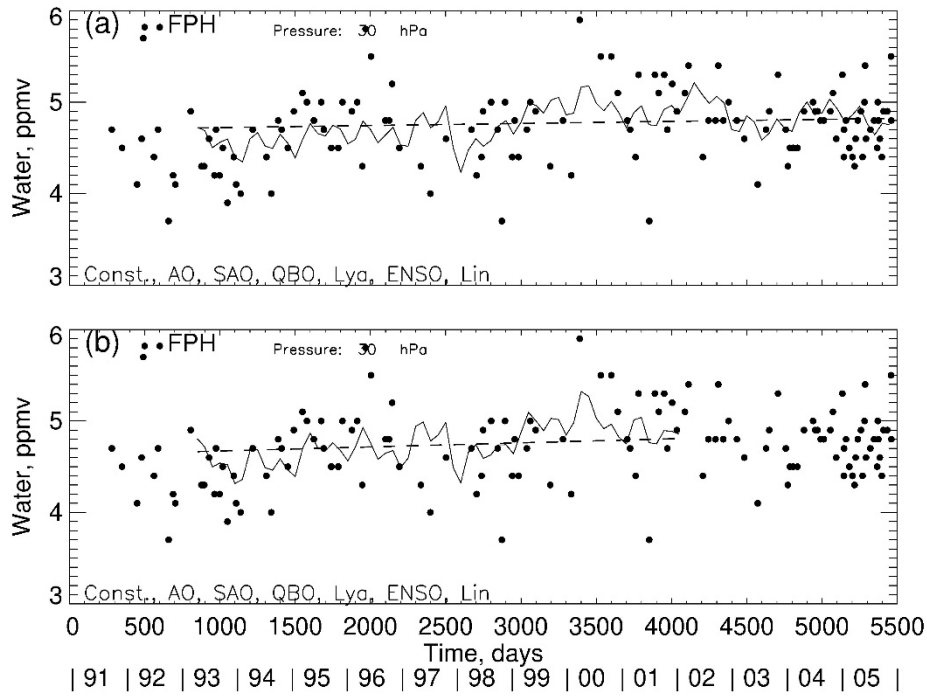


337

338 Figure 2—Residual from MLR model fit to HALOE time series data of Fig. 1(a).

339

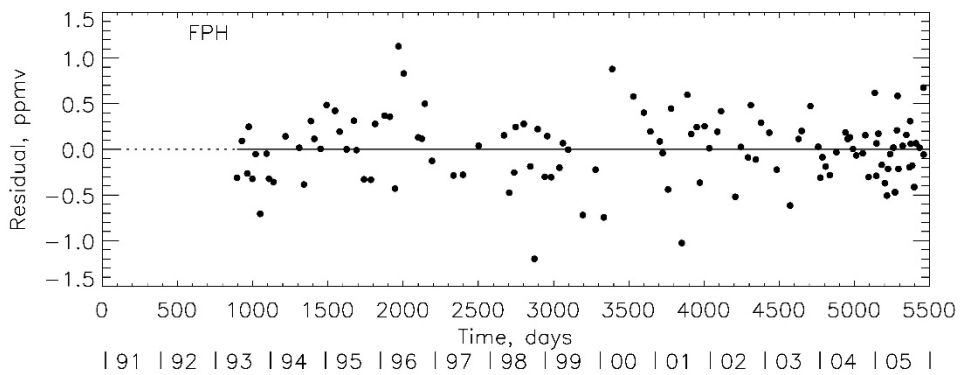
340



341

342 Figure 3—Time series of FPH data and MLR fit to them for comparison with Fig. 1; (a) 1993-  
343 2005, (b) 1993-2002.

344



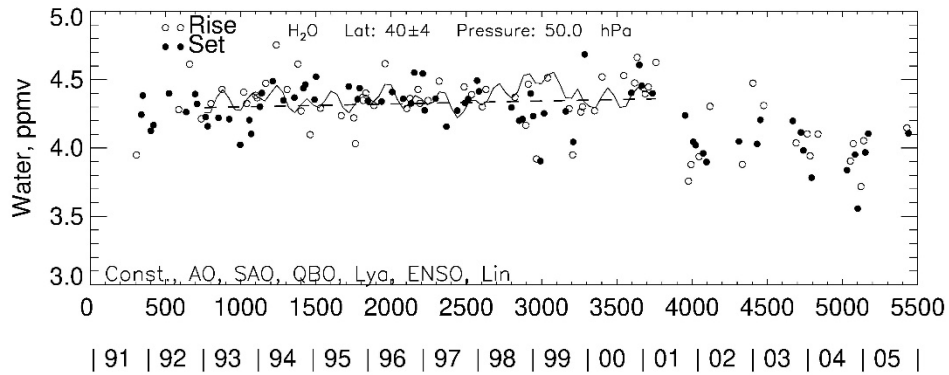
345

346 Figure 4—Time series residual for the MLR fit to the FPH data of Fig. 3(a).

347

348

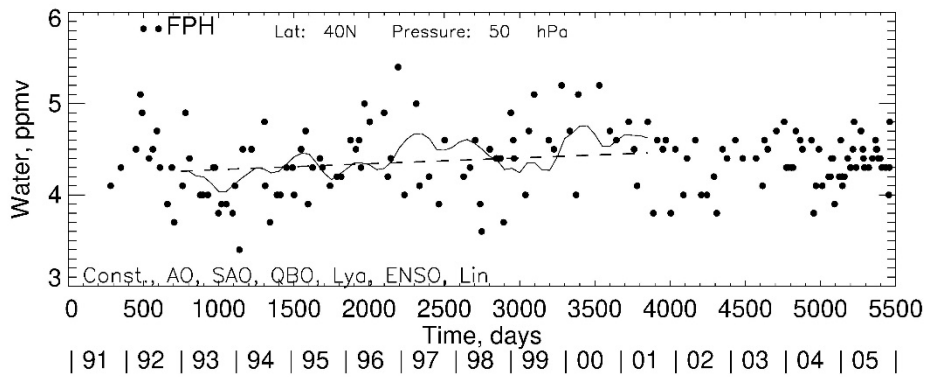
349



350

351 Figure 5—HALOE time series data at 50 hPa and MLR fit to them for 1993 to 2002.

352



353

354 Figure 6—As in Fig. 5, but for FPH data.

355

356

357

358

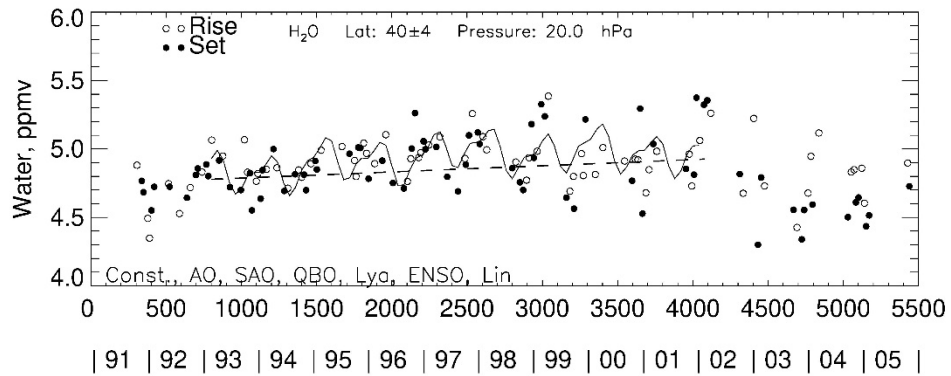
359

360

361

362

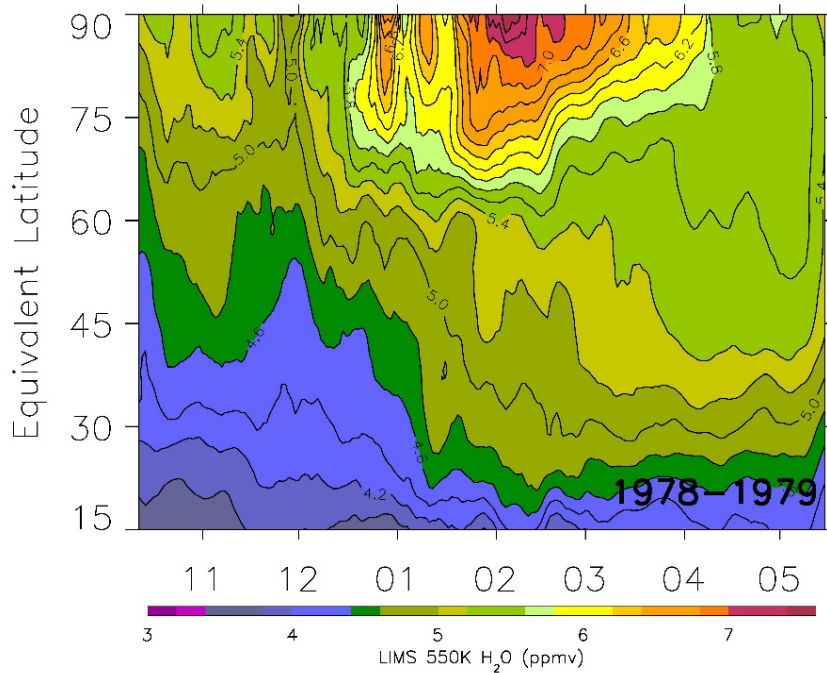
363



364

365 Figure 7— HALOE time series data at 20 hPa and MLR fit to them for 1993 to 2002.

366



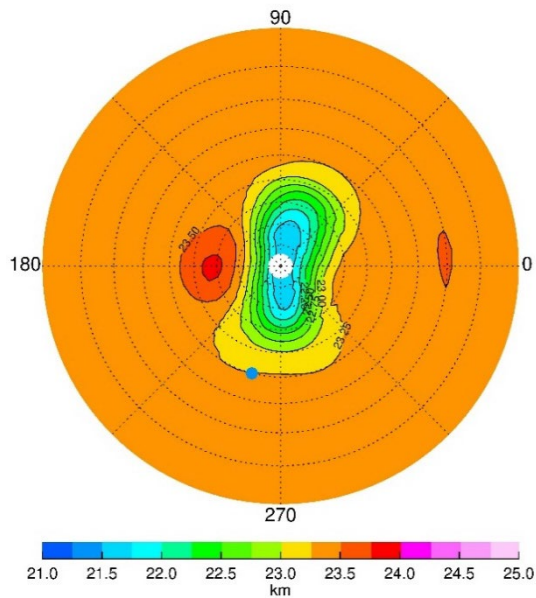
367

368 Figure 8—Time series of LIMS water vapor vs. equivalent latitude at 550 K and with smoothing  
369 over 7 days. Contour interval is 0.2 ppmv. Tic marks along the abscissa denote the middle of  
370 each month.

371



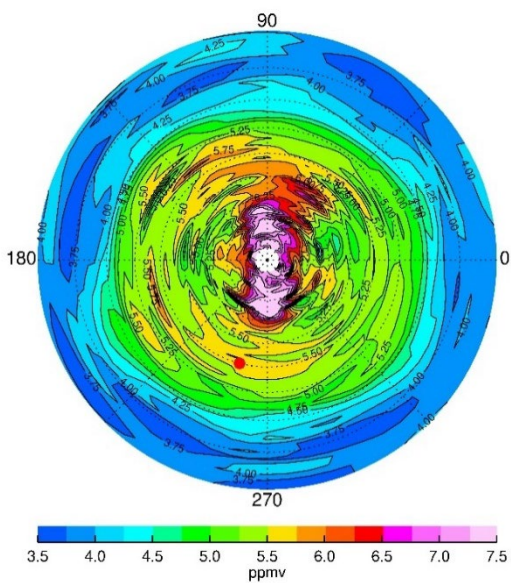
372



373

374 Figure 9—NH plot on the 31.6-hPa surface for 17 February 1979 of LIMS geopotential height  
375 (GPH). Contour increment for GPH is 0.25 gpkm, and dashed circles are at every 10° of  
376 latitude. Blue dot is location of Boulder, CO (40°N, 255°E).

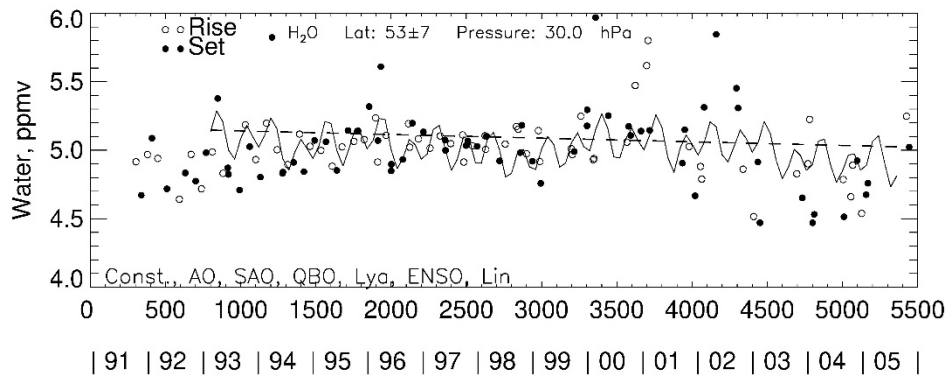
377



378

379 Figure 10—As in Fig. 9, but for LIMS SWV on 17 February. Contour interval (CI) is 0.25  
380 ppmv. Red dot is location of Boulder.

381



382

383 Figure 11—As in Fig. 1(a), but for a European sector, centered at 53°N, 35°E.

384

385

386 **References**

387 Bhatt, P. P., Remsberg, E. E., Gordley, L. L., McInerney, J. M., Brackett, V. G., and Russell III,  
388 J. M.: An evaluation of the quality of Halogen Occultation Experiment ozone profiles in the  
389 lower stratosphere, *J. Geophys. Res.*, 104, <https://doi.org/10.1029/1999JD900058>, 1999.

390

391 Charlton, A. J., and Polvani, L. M.: A New Look at Stratospheric Sudden Warmings. Part I:  
392 Climatology and Modeling Benchmarks, *J. Climate*, 20, <https://doi.org/10.1175/JCLI3996.1>,  
393 2007.

394

395 Curbelo, J., Chen, G., & Mechoso, C. R.: Lagrangian analysis of the northern stratospheric polar  
396 vortex split in April 2020. *Geophys. Res. Lett.*, 48, e2021GL093874.

397 <https://doi.org/10.1029/2021GL093874>, 2021.

398

399 Davis, S. M., Rosenlof, K. H., Hassler, B., Hurst, D. F., Read, W. G., Vömel, H., Selkirk, H.,  
400 Fujiwara, M., and Damadeo, R.: The stratospheric water and ozone satellite homogenized  
401 (SWOOSH) database: a long-term database for climate studies, *Earth Syst. Sci. Data*, 8, 461-490,  
402 [www.earth-syst-sci-data.net/8/461/2016/doi:10.5194/essd-8-461-2016](http://www.earth-syst-sci-data.net/8/461/2016/doi:10.5194/essd-8-461-2016), 2016.

403

404 Gordley, L. L., Thompson, E., McHugh, M., Remsberg, E., Russell III, J., and Magill, B.:  
405 Accuracy of atmospheric trends inferred from the Halogen Occultation Experiment data, *J. Appl.*  
406 *Remote Sensing*, 3, <https://doi.org/10.1117/1.3131722>, 2009.

407

408 Hall, E. G., Jordan, A. F., Hurst, D. F., Oltmans, S. J., Vömel, H., Kühnreich, B., and Ebert, V.:  
409 Advancements, measurement uncertainties, and recent comparisons of the NOAA frost point  
410 hygrometer, *Atmos. Meas. Tech.*, 9, <https://doi.org/10.5194/amt-9-4295-2016>, 2016.

411

412 Harries, J. E., Russell III, J. M., Tuck, A. F., Gordley, L. L., Purcell, P., Stone, K., Bevilacqua,  
413 R. M., Gunson, M., Nedoluha, G., and Traub, W. A.: Validation of measurements of water vapor

414 from the Halogen Occultation Experiment (HALOE), *J. Geophys. Res.*, 101,  
415 <https://doi.org/10.1029/95JD02933C>, 1996.

416

417 Hegglin, M. I., Plummer, D. A., Shepherd, T. G., Scinocca, J. F., Anderson, J., Froidevaux, L.,  
418 Funke, B., Hurst, D., Rozanov, A., Urban, J., von Clarmann, T., Walker, K. A., Wang, H. J.,  
419 Tegtmeier, S., and Weigel, K.: Vertical structure of stratospheric water vapour trends derived  
420 from merged satellite data, *Nature Geoscience*, 7(10), 768–776.  
421 <https://doi.org/10.1038/NGEO2236>, 2014.

422

423 Hervig, M. E., Russell III, J. M., Gordley, L. L., Park, J. H., Drayson, S. R., and Deshler, T.:  
424 Validation of aerosol measurements from the Halogen Occultation Experiment, *J. Geophys. Res.*,  
425 101, <https://doi.org/10.1029/95JD02464>, 1996.

426

427 Hervig, M. E., Russell III, J. M., Gordley, L. L., Daniels, J., Drayson, S. R., Park, J. H.: Aerosol  
428 effects and corrections in the Halogen Occultation Experiment, *J. Geophys. Res.*, 100,  
429 <https://doi.org/10.1029/94JD02143>, 1995.

430

431 Hurst, D. F., Oltmans, S. J., Vömel, H., Rosenlof, K. H., Davis, S. M., Ray, E. A., Hall, E. G.,  
432 and Jordan, A. F.: Stratospheric water vapor trends over Boulder, Colorado: Analysis of the 30  
433 year Boulder record, *J. Geophys. Res.*, 116, <https://doi.org/10.1029/2010JD015065>, 2011.

434

435 Konopka, P., Tao, M., Ploeger, F., Hurst, D. F., Santee, M. L., Wright, J. S., and Riese, M.:  
436 Stratospheric moistening after 2000, *Geophysical Research Letters*, 49, e2021GL097609.  
437 <https://doi.org/10.1029/2021GL097609>, 2022.

438

439 Lossow, S., Hurst, D. F., Rosenlof, K. H., Stiller, G. P., von Clarmann, T., Brinkop, S., Dameris,  
440 M., Jöckel, P., Kinnison, D. E., Pliening, J., Plummer, D. A., Ploeger, F., Read, W. G.,  
441 Remsberg, E. E., Russell III, J. M., and Tao, M.: Trend differences in lower stratospheric water

442 vapour between Boulder and the zonal mean and their role in understanding fundamental  
443 observational discrepancies, *Atmos. Chem. Phys.*, 18, 8331-8351, [https://doi.org/10.5194/acp-](https://doi.org/10.5194/acp-18-8331-2018)  
444 [18-8331-2018](https://doi.org/10.5194/acp-18-8331-2018), 2018.

445

446 Manney, G. L., Millan, L. F., Santee, M. L., Wargan, K., Lambert, A., Neu, J. L., Werner, F.,  
447 Lawrence, Z. D., Schwartz, M. J., Livesey, N. J., and Read, W. G.: Signatures of Anomalous  
448 Transport in the 2019/2020 Arctic Stratospheric Polar Vortex, *J. Geophys. Res. Atmospheres*,  
449 127, e2022JD037407, <https://doi.org/10.1029/2022JD037407>, 2022.

450

451 Randel, W. J., Wu, F., Vömel, H., Nedoluha, G. E., and Forster, P.: Decreases in stratospheric  
452 water vapor after 2001: Links to changes in the tropical tropopause and the Brewer-Dobson  
453 circulation, *J. Geophys. Res. Atmospheres*, 111, <https://doi.org/10.1029/2005JD006744>, 2006.

454

455 Remsberg, E.: Methane as a diagnostic tracer of changes in the Brewer-Dobson circulation of the  
456 stratosphere, *Atmos. Chem. Phys.*, 15, 3739-3754, <https://doi.org/10.5194/acp-15-3739-2015>,  
457 2015.

458

459 Remsberg, E. E.: On the response of Halogen Occultation Experiment (HALOE) stratospheric  
460 ozone and temperature to the 11-yr solar cycle forcing, *J. Geophys. Res.-Atmospheres*, 113,  
461 <https://doi.org/10.1029/2008JD010189>, 2008.

462

463 Remsberg, E., Damadeo, R., Natarajan, M., and Bhatt, P.: Observed responses of mesospheric  
464 water vapor to solar cycle and dynamical forcings, *J. Geophys. Res.*, 123, 3830-3843,  
465 <https://doi.org/10.1002/2017JD028029>, 2018a.

466

467 Remsberg, E., Natarajan, M., and Harvey, V. L.: On the consistency of HNO<sub>3</sub> and NO<sub>2</sub> in the  
468 Aleutian High region from the Nimbus 7 LIMS Version 6 dataset, *Atmos. Meas. Tech.*, 11,  
469 3611-3626, <https://doi.org/10.5194/amt-11-3611-2018>, 2018b.

470

471 Scherer, M., Vömel, H., Fueglistaler, S., Oltmans, S.J., and Staehelin, J.: Trends and variability  
472 of midlatitude stratospheric water vapour deduced from the re-evaluated Boulder balloon series  
473 and HALOE, *Atmos. Chem. Phys.*, 8, 1391–1402, [www.atmos-chem-phys.net/8/1391/2008/](http://www.atmos-chem-phys.net/8/1391/2008/),  
474 2008.

475

476 *SPARC Report No. 8 of the SPARC Data Initiative: Assessment of stratospheric trace gas and*  
477 *aerosol climatologies from satellite limb sounders*, Prepared by the SPARC Data Initiative Team  
478 and edited by M. I. Hegglin and S. Tegtmeier, WCRP-5/2017, Geneva,  
479 <https://doi.org/10.3929/ethz-a-010863911>, 2017.

480

481 Tiao, G. C., Reinsel, G. C., Xu, D., Pedrick, J. H., Zhu, X., Miller, A. J., DeLuisi, J. J., Mateer,  
482 C. L., and Wuebbles, D. J.: Effects of autocorrelation and temporal sampling schemes on  
483 estimates of trend and spatial correlation, *J. Geophys. Res.*, 95, 20507–20517,  
484 <https://doi.org/10.1029/JD095iD12p20507>, 1990.

485

486 Wargan, K., Weir, B., Manney, G. L., Cohn, S. E., Knowland, K. E., Wales, P. A., and Livesey,  
487 N. J.: M2-SCREAM: A stratospheric composition reanalysis of Aura MLS data with MERRA-2  
488 transport. *Earth and Space Science*, 10, e2022EA002632.,  
489 <https://doi.org/10.1029/2022EA002632>, 2023.

490